Robotica (1999) volume 17, pp. 335–342. Printed in the United Kingdom © 1999 Cambridge University Press

Dynamic balancing of hexapods for high-speed applications

F. Xi

Integrated Manufacturing Technologies Institute, National Research Council Canada, London, Ontario, (Canada) N6G 4X8
E-mail: jeff.xi@nrc.ca

(Received in Final Form: January 12, 1999)

SUMMARY
In this paper, a method is proposed for dynamic balancing of hexapods for high-speed applications. The kinematic structure of the hexapod is based on the parallel mechanism. For high-speed applications, hexapod dynamics is the dominant factor, and dynamic balancing becomes very important. The proposed method is aimed at minimizing the changes in the hexapod inertia over the workspace by utilizing the tool holder attached to the hexapod's end-effector as a counterweight.

KEYWORDS: Hexapods; Dynamic balancing; High-speed applications; Tool holder.

1. INTRODUCTION

The conventional machine tools have been built based on stacking motion systems, such as x-y tables, and as such the bottom motion system has to carry the weight of the motion systems on the top. Due to this stacking nature, the traveling speeds of the conventional machine tools are limited. While research is being carried out on utilization of lightweight materials to reduce the weight of the motion systems, new machine tools are being developed based on unconventional machine kinematics. Two types of machine have emerged, namely, *gate structure* and *hexapod*. In a gate structure, the actuators are placed on a gantry to withstand the weight while driving other passive mechanisms, such as scissors or gate shifters, which in turn provide the motions in the required directions.[1]

The hexapod is based on the parallel closed-chain kinematic structure known as the Stewart platform.[2] This structure has already been used in various applications, for instance, flight simulator,[3] telescope tip tilting system[4] and micro biological manipulator.[5] Compared to the conventional machine tools, the parallel mechanism structure offers superior stiffness, lower mass and higher acceleration. While repeatability and tracking accuracy are maintained at the same level, the maximum feedrate and acceleration of the hexapod machine tool can now reach about 100m/min of velocity and 1–2g of acceleration, respectively,[6] a substantial increase from about 30m/min of velocity and 0.3g of acceleration of the conventional machine tools. Moreover, hexapods have the potential to be highly reconfigurable and modular, with other advantages including higher dexterity, simpler and fewer fixtures, and multi-mode manufacturing capabilities. Also, it can be shown that the hexapod machine tool has reduction or even cancellation effect of the leg errors on the hexapod location accuracy.[7]

Research in the parallel mechanism can be categorized in two areas: mechanical design and control design. Mechanical design of a hexapod involved kinematic structure design combined with kinematics and dynamics analysis. Kinematic structure design of a parallel mechanism is a classic problem, and has been studied extensively, as summarized by Hunt,[8] and Earl and Rooney.[9] There are a number of ways to classify the parallel mechanism. Here, we are interested in joint actuations, and in this regard, the parallel mechanism structure may be classified as *prismatic* or *revolute*. The commercially available hexapods, as listed in Table I, are mainly prismatic type, called servo-struts, which use servo-motors to drive and control ball screws to provide linear motions along the legs. New servo systems utilizing linear direct drives are being explored.[10] Though revolute joints are not seen in the commercial hexapods, research is being carried out. For example, a three degrees-of-freedom hexapod, called DELTA, was developed in Switzerland, and later modified as a six degree-of-freedom hexapod, called HEXA in France[11] for high-speed applications. In these two prototypes, each leg is made of a two-link manipulator with the first joint attached to the base under actuation while the second joint as a passive joint. Besides pure prismatic or revolute joint actuation, hybrid design of combining the two was discussed by Behi[12] and Tsai.[13]

Table I. Commercial hexapods.

Machine	Maker	Acceleration, Velocity, Repeatability
VARIAX	Giddings & Lewis, Inc.	1 g, 66m/min, 11μm.
Octahedral Hexapod	Ingersoll Milling Machine Co.	0.5g, 40m/min, ~10μm.
Tornado 2000	Hexel Corp.	0.5–1.5g, 15–25m/min, 10μm.
HexaM	Toyoda Machine Works Ltd.	1.2g, 100/m/mim, 10μm.
Geodetic Hexapod	Geodetic	1g, 40m/min, ~10μm.
TM	LAPIK	1g, 15m/min, Not available

https://doi.org/10.1017/S0263574799001484 Published online by Cambridge University Press

As for the kinematics and dynamics analysis of the parallel mechanism, a great deal of research has been carried out, resulting in a very rich literature. Due to the space limitation, only a few representative methods are mentioned here. For example, the Plücker line coordinates[14] and motor algebra[15] were introduced for the kinematic and dynamic analysis of the parallel manipulator. The Grassmann geometry[16] was applied to analyze the singular configurations of the parallel manipulator. The methods based on the optimization theory were developed to improve the kinematic performance of the parallel manipulator, such as workspace maximization and kinematic isotropy.[7] A modified design method was proposed by Stoughton and Arai[18] to increase the dexterity of the parallel mechanism by placing the legs of parallel manipulator on two concentric circles.

In terms of the parallel mechanism control, there are two basic methods, namely, non model-based control, such as PID,[19] and model-based control, such as computed torques.[20] The former is effective for most position control applications but not adequate for tracking control operations, and hence the latter was developed for more precise control. Two approaches used in the model-based control of the closed-chain mechanisms are *linearized* and *non-linear*.[21] In the first approach, the parallel mechanism is modeled as a linear system and controlled by an adaptive control method. In the second approach, control inputs are determined based on a full dynamic model. The linearized approach may have stability problem while the non-linear approach does not.[21]

Due to the fact that hexapods are used for high-speed applications, the hexapod dynamics becomes the dominant factor and dynamic balancing is of particular importance. Dynamic balancing will not only improve the hexapod dynamic performance by reducing the disturbance due to dynamic force variation, but also enhance the control system, especially for the linear direct drive that is very sensitive to dynamic force variation.[10] Walker[21] pointed out that a linearized system could perform satisfactorily if the dynamic parameters are not subject to rapid change. Upon achieving dynamic balancing, dynamic change is minimized and hence a hexapod may be well under a linearized control, thereby simplifying the control system.

In this paper, the problem of hexapod dynamic balancing is the first time addressed. A method is proposed aiming at minimizing the changes in the hexapod dynamic forces over the workspace by utilizing the tool holder attached to the hexapod's end-effector as a counterweight. To describe the proposed method, the rest of the paper is organized as follows. Kinematic and dynamic formulation is described in Section 2, dynamic balancing in Section 3, balancing methodology in Section 4, and case studies in Section 5. The paper concludes at Section 6.

2. KINEMATIC AND DYNAMIC FORMULATION

2.1 Kinematic structure

The hexapod under consideration is a six degrees-of-freedom prismatic type of parallel mechanism, as shown in Figure 1. In this structure, each leg is driven linearly along its axis, with one end fixed in the base and the other end fixed in the moving platform. The mobility of the mechanism can be examined by the following equation[8]

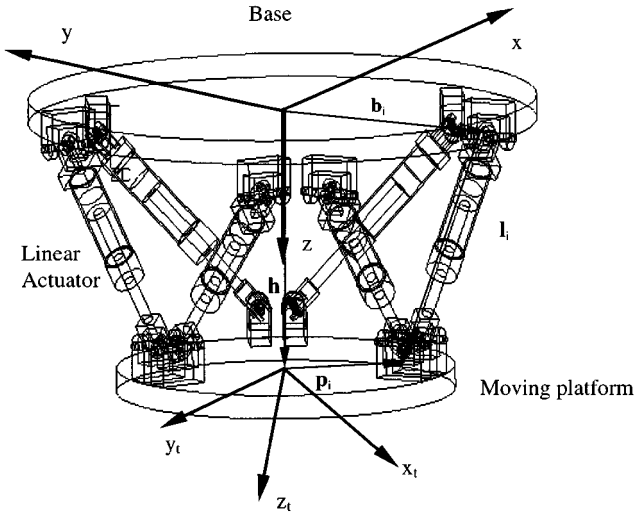

Fig. 1. Schematic of a six degree-of-freedom prismatic hexapod.

$$M = d(n - g - 1) + \sum_{i=1}^{g} f_i \tag{1}$$

where M denotes the mobility, or the effective degrees-of-freedom, d is the order of the system ($d = 3$ for planar motion, and $d = 6$ for spatial motion), n is the number of the links including the frame, g is the number of joints, and f_i is the number of degrees-of-freedom for the ith joint. For a six degree-of-freedom hexapod, M is 6 and d is 6. For the prismatic structure, n is 14, as each leg consists of two links with one fixed and another sliding, in total 12, plus the base and the moving platform. If each leg has its own connection with the base and the moving platform then there are 18 joints, that is 12 connection joints and 6 prismatic joints. By substituting $M = 6$, $d = 6$, $n = 14$ and $g = 18$ into equation (1), it can be seen that the required joint degrees-of-freedom for each leg is 6. Excluding the prismatic joint (1 d.o.f.), then for each leg one connecting joint should be spherical (3 d.o.f.) and another should be universal (2 d.o.f.), which is the case under this study. The prismatic joints are active, whereas the connecting joints are passive joints. For high-speed applications, the passive joints are very critical in terms of friction, as excessive friction generates heat, which may degrade machine performance or even damage the machine in the worst case. New anti-friction joints, such as hydrostatic and magnetic, are under development.[22]

2.2 Kinematic equations

The leg kinematic equations of a hexapod are formulated by considering closed kinematic loops. For the ith loop as shown in Figure 1, the following relationship holds

$$\mathbf{l}_i = \mathbf{h} + \mathbf{p}_i - \mathbf{b}_i \qquad \text{for } i = 1,6 \tag{2a}$$

where $\mathbf{L}_i$ is the leg vector, $\mathbf{h}$ is the translation vector between

https://doi.org/10.1017/S0263574799001484 Published online by Cambridge University Press

the base and the moving platform, $\mathbf{p}_i$ is the position vector of the ith leg's joint attached to the moving platform, and $\mathbf{b}_i$ is the position vector of the ith leg's joint attached to the base platform, and these vectors are expressed in global coordinates O-xyz. In terms of the rotation matrix $\mathbf{R}$ between the base and the moving platform, vector $\mathbf{p}_i$ can be expressed as $\mathbf{p}_i = \mathbf{R}\ {}^t\mathbf{p}_i$, where superscript t indicates a vector with respect to the coordinate frame on the moving platform O-$x_t y_t z_t$. Substituting the rotation matrix form into equation (2a) yields

$$\mathbf{l}_i = \mathbf{h} + \mathbf{R}\ {}^t\mathbf{p}_i - \mathbf{b}_i \tag{2b}$$

The leg displacement equations are obtained by taking the norm of equation (2b) as

$$q_i = \| = \| \mathbf{L}_i \| \mathbf{h} + \mathbf{R}\ {}^t\mathbf{p}_i - \mathbf{b}_i \| \tag{3a}$$

For given parallel mechanism structure, $\mathbf{b}_i$ and ${}^t\mathbf{p}_i$ are both determined, and only variables in equation (3a) are $\mathbf{h}$, $\mathbf{R}$, and q_i. The translation vector $\mathbf{h}$ contains three scalar variables, representing three linear movements. The rotation matrix $\mathbf{R}$ can be shown to have three independent scalar variables in terms of $tr(\mathbf{R})$ and $vect(\mathbf{R})$.[23] Hence, equation (3a) represents a set of non-linear equations with six knowns and six unknowns, and can be re-written in a symbolic form as

$$\mathbf{q} = \boldsymbol{f}(\mathbf{x}) \tag{3b}$$

where $\mathbf{q} = [q_1, q_2, \ldots q_6]^T$, and $\mathbf{x} = [\mathbf{x}_p, \mathbf{x}_o]^T$, $\mathbf{x}_p$ and $\mathbf{x}_o$ are the vectors presenting the hexapod's position and orientation, respectively, and they are determined from $\mathbf{R}$ and $\mathbf{h}$. For given translation vector $\mathbf{h}$ and rotation matrix $\mathbf{R}$, $\mathbf{q}$ can be determined by the inverse kinematics, which is straighforward. The forward kinematics, i.e. to determine $\mathbf{R}$ and $\mathbf{h}$ for given leg displacements $\mathbf{q}$, is relatively difficult.[24] Additional angle sensors are useful to solve this problem.[25]

Taking time derivative of equation (2b) yields the leg velocity vector

$$\dot{\mathbf{L}}_i = \mathbf{v} + \omega \times \mathbf{R}\ {}^t\mathbf{p}_i \tag{4a}$$

where $\mathbf{v}$ and ω are the linear and angular velocity of the moving platform, and the leg velocity is obtained by projecting the leg velocity vector on to the leg unit vector

$$\dot{q}_i = \mathbf{e}_i^T \dot{\mathbf{L}}_i \tag{4b}$$

where $\mathbf{e}_i$ is the unit vector of the ith leg and given by $\mathbf{e}_i = \mathbf{l}_i / q_i$. The leg acceleration vector is given by taking time derivative of equation (4a)

$$\ddot{\mathbf{L}}_i = \dot{\mathbf{v}} + \dot{\boldsymbol{\omega}} \times \mathbf{R}^t\mathbf{P}_i + \boldsymbol{\omega} \times (\boldsymbol{\omega} \times \mathbf{R}^t\mathbf{p}_i) \tag{5a}$$

Subsequently, the leg acceleration equals

$$\ddot{q}_i = \mathbf{e}_i^T \ddot{\mathbf{L}}_i \tag{5b}$$

2.3 Dynamic equations

The dynamic equations of the hexapod are presented here for the moving platform, as leg mass is usually considered negligible. Discussion on full dynamics including leg mass can be found in reference 26. In light of the Lagrange formulation, the Lagrangian of the moving platform can be written as

$$\mathfrak{L} = \frac{1}{2} \dot{\mathbf{x}}^T \mathbf{M} \dot{\mathbf{x}} - m\mathbf{g}^T\mathbf{h} \tag{6}$$

where $\dot{\mathbf{x}} = [\omega^T\ \mathbf{v}^T]^T$, $\mathbf{g}$ is the gravitational acceleration vector, and $\mathbf{M}$ is the inertia matrix in terms of the moment of inertia $\mathbf{I}$ and the mass m of the moving platform, i.e.

$$\mathbf{M} = \begin{bmatrix} \mathbf{I} & 0 \\ o & m\mathbf{1} \end{bmatrix}$$

To relate the Lagrangian to the actuator coordinates, the instantaneous kinematics is used, that is

$$\dot{\mathbf{q}} = \mathbf{J}\dot{\mathbf{x}} \tag{7}$$

where $\dot{\mathbf{q}} = [\dot{q}_1\ \dot{q}_2 \ldots \dot{q}_6]^T$ and $\mathbf{J}$ is the Jacobian defined as

$$\mathbf{J}^T = \begin{bmatrix} \mathbf{R}\,{}^t\mathbf{p}_1 \times \mathbf{e}_1 & \mathbf{R}\,{}^t\mathbf{p}_2 \times \mathbf{e}_2 & \ldots & \mathbf{R}\,{}^t\mathbf{p}_6 \times \mathbf{e}_6 \\ \mathbf{e}_1 & \mathbf{e}_2 & \ldots & \mathbf{e}_6 \end{bmatrix} \tag{8}$$

In light of equation (7), the Lagrangian can be re-written in terms of the actuator coordinates as

$$\mathfrak{L} = \frac{1}{2} \dot{\mathbf{q}}^T \mathbf{D}\, \dot{\mathbf{q}} - m\, \mathbf{g}^T\mathbf{h} \tag{9}$$

where $\mathbf{D}$ is the generalized inertia matrix defined as

$$\mathbf{D} = (\mathbf{J}^{-1})^T \mathbf{M}\, \mathbf{J}^{-1} \tag{10}$$

In terms of $\mathbf{D}$, the equations of the motion of the hexapod can be obtained as

$$\mathbf{D}\ddot{\mathbf{q}} + \mathbf{C}(\dot{\mathbf{q}}, \mathbf{q}) + \mathbf{G} = \mathbf{u} \tag{11}$$

where $\mathbf{u} = [u_1, u_2, \ldots u_6]^T$ is the vector of the actuator forces, $\mathbf{G}$ is the gravitational term, and $\mathbf{C}$ is defined as

$$\mathbf{C} = \left(\sum_{i=1}^{6} \frac{\partial \mathbf{D}}{\partial q_i} \right) \dot{\mathbf{q}} - \frac{\mathbf{1}}{\mathbf{2}} \text{col.} \left[\dot{\mathbf{q}}^T \frac{\partial \mathbf{D}}{\partial q_1} \dot{\mathbf{q}}, \ldots \dot{\mathbf{q}}^T \frac{\partial \mathbf{D}}{\partial q_6} \dot{\mathbf{q}} \right] \tag{12}$$

where *col.*[] denotes a column vector.

3. DYNAMIC BALANCING

3.1 Generalized inertia ellipsoid (GIE)

Since hexapods are designed to operate at high speeds, system dynamics becomes very important. As can be seen from equation (11), the dynamic equations of the hexapod are coupled, non-linear and configuration-dependent. Coupling effect appears both in $\mathbf{D}$, inertia term, and $\mathbf{C}$, the centrifugal and Coriolis terms, indicating that the inertia, centrifugal and Coriolis forces in different directions affect each other. Non-linearity is present also in $\mathbf{D}$ and $\mathbf{C}$, as it can be noted that $\mathbf{D}(\mathbf{q})$ is configuration-dependent and $\mathbf{C}(\dot{\mathbf{q}}, \mathbf{q})$ is configuration and velocity-dependent. For high speed applications, due to increased speed and acceleration, the inertia, centrifugal and Coriolis forces become very large, and if not balanced, could degrade hexapod's performance.

https://doi.org/10.1017/S0263574799001484 Published online by Cambridge University Press

For the past twenty years or so, research has been carried out on balancing of parallel mechanisms. There are two types of balancing, namely, *static balancing* and *dynamic balancing*. Static balancing is to balance the gravity so that the weight of the machine components does not produce any force or torque at the actuators under static conditions. Raghavan and Roth[27] proposed a design methodology for parallel manipulators based on static balancing. Stoughton and Arai[18] presented a modified design of the Stewart platform by introducing two concentric circles both at the base and at the end effector, and showed improvement in static balancing. Jean and Gosselin[28] studied the problem of static balancing of planar parallel manipulators, and derived the balancing conditions for one, two and three degrees-of-freedom of planar parallel manipulators.

Dynamic balancing is to balance the inertia so that the dynamic force change could be cancelled or minimized. The focus in this area, however, has been on dynamic balancing of four bar linkages. In general, it is possible to completely balance the dynamic force of four bar linkages,[29] whereas it is difficult to balance the dynamic moment and additional mechanisms, such as idler loops, may be needed.[30] Till now, the problem of dynamic balancing of spatial parallel mechanisms has not been investigated. This problem is of particular importance for hexapods under high-speed applications. Nevertheless, research on minimization of inertia change has been studied for the serial manipulators, as summarized by Singh and Rastegar.[31] The approach is to find an optimal generalized inertia matrix **D** as close to isotropy and constancy as possible. This idea is adopted here for dynamic balancing of hexapods. Prior to describing the proposed method for hexapod dynamic balancing, the concept about isotropy and constancy is reviewed.

3.2 Isotropy

Isotropy can be defined by the generalized inertia ellipsoid (GIE).[32] Denote by λ_i the ith eigenvalue, and by $\mathbf{a}_i$ the ith eigenvector of **D** ($i = 1, 6$), the direction of the ith axis of the GIE is defined by $\mathbf{a}_i$ and the length is equal to $1/\sqrt{\lambda_i}$. Isotropy is referred to as a sphere GIE, i.e. all the axis lengths are equal, and in this case, the dynamic forces are de-coupled. To measure isotropy of **D**, an anti-isotropy measure[31] can be used

$$\sigma(\mathbf{D}) = \frac{1}{\sqrt{\kappa(\mathbf{D})}} = \sqrt{\frac{\lambda_n}{\lambda_1}} \tag{13}$$

where $\kappa(\mathbf{D})$ is the condition number of **D**, λ_1 and λ_n are the maximum and minimum eigenvalue of **D**, respectively. GIE is isotropic when $\sigma = 1$, and is not when $\sigma < 1$. Since $\sigma \leq 1$, maximization of σ means closer to isotropy. As for the size of GIE, it can be measured by

$$\gamma(\mathbf{D}) = \tfrac{1}{2n}\sqrt{\frac{1}{det(\mathbf{D})}} = \tfrac{1}{2n}\sqrt{\frac{1}{(\lambda_1 \cdot \lambda_2 \ldots \lambda_n)}} \tag{14}$$

where $det(\mathbf{D})$ is the determinant of **D**. As shown by Asada,[32] $\gamma(\mathbf{D})$ is related to the inverse of the square root of the average generalized moment of inertia, and hence maximization of $\gamma(\mathbf{D})$ will reduce the hexapod inertia. Another isotropy measure introduced by Ma and Angeles[33] is the dynamic condition index (DCI)

$$\|\mathbf{B}\|_F = \frac{1}{2}\mathbf{b}^T\mathbf{W}\mathbf{b} \tag{18}$$

where subscript F denotes the Frobenius norm, and **b** is the vector composed of the upper triangular components of **B** defined as $\mathbf{B} = \mathbf{D}(\mathbf{q}) - \mu\mathbf{1}$, $\mu = tr(\mathbf{D})/6$, and **W** is the diagonal weighting matrix that can be selected based on the relative relevance between entries of **D**. Minimization of DCI is closer to isotropy.

3.3 Constancy

Constancy means that matrix **D** is invariant within the workspace. It can be seen from equation (12) that if **D** does not vary with **q**, i.e. $\partial\mathbf{D}/\partial\mathbf{q}$, then $\mathbf{C} = \mathbf{0}$, indicating that there will be no non-linear forces from centrifugal and Coriolis terms. It was shown in reference 32 that change in **D** could be expressed in terms of changes in λ_i and $\mathbf{a}_i$, that is

$$\delta\mathbf{D} = \begin{bmatrix} \delta\lambda_1 & (\lambda_1 - \lambda_2)\delta\phi_{12} & \ldots & (\lambda_1 - \lambda_n)\delta\phi_{1n} \\ (\lambda_1 - \lambda_2)\delta\phi_{12} & \delta\lambda_2 & \ldots & \ldots \\ \vdots & \vdots & \vdots & \vdots \\ (\lambda_1 - \lambda_n)\delta\phi_{1n} & \ldots & \ldots & \delta\lambda_n \end{bmatrix} \tag{15}$$

where ϕ_{ij} is the angle between $\mathbf{a}_i$ and $\mathbf{a}_j$. Two constancy measures were introduced in reference 34 in terms of changes in λ_i and $\mathbf{a}_i$ with respect to **q**. The first measure is defined by the Euclidean norm of the eigenvalue derivatives

$$\tau_1 = \left\| \frac{\partial\boldsymbol{\lambda}}{\partial\mathbf{q}} \right\| \tag{16}$$

where $\lambda = [\lambda_1, \lambda_2, \ldots \lambda_6]^T$. The second measure is expressed as

$$\tau_2 = \left\| \mathbf{A}^T \boldsymbol{\Sigma} \frac{\partial\mathbf{A}}{\partial\mathbf{q}} \right\| \tag{17}$$

where $\mathbf{A} = [\mathbf{a}_1, \mathbf{a}_2, \ldots \mathbf{a}_6]$, and $\Sigma = \mathrm{diag}(\lambda_i)$.

4. BALANCING METHODOLOGY

4.1 The global dynamic characteristics

As mentioned in the previous section, the measures of isotropy and constancy are function of the actuator configurations **q**. In order to minimize the change in **D**, a global dynamic measure is needed, and it may be formulated by considering a task function of the hexapod. When a hexapod is assigned to a specific task, it is possible to specify a task function in the global coordinates **x** in terms of the number of visitations to a region,[31] for example

https://doi.org/10.1017/S0263574799001484 Published online by Cambridge University Press

$$p(\mathbf{x}) = \frac{n_i}{N} \quad \text{if } \mathbf{x} \in \Omega_i,\ i = 1, K \tag{18}$$

where $p(\mathbf{x})$ represents a probability function n_i indicates the number of visitations to region Ω_i, N is the total number of visitations, and K is the total number of regions. Note from equation (3b) that $\mathbf{x}$ and $\mathbf{q}$ are related by the hexapod kinematics.

With the probability function $p(\mathbf{x})$, a global dynamic measure can be defined based on an equivalent probabilistic model. Denote by GDI a global dynamic index, it can be selected from the indices given in Section 3 or their combinations, depending on the nature of the problem. For example, if the dynamic condition index (DCI) is chosen as the GDI, then GDI $\equiv$ DCI.

Upon selection of a GDI, the statistical parameters, such as commonly used mean value and standard deviation can be obtained using the probability theory. The mean value may be interpreted as a middle point of the GDI over the regions considered, and the standard deviation as the fluctuation of the GDI relative to the middle point. If necessary, higher order statistical parameters can also be used. In the paper, we limit ourselves to the mean value and standard deviation.

4.2 Dynamic balancing using optimization

To this end, the problem of hexapod dynamic balancing may be more specifically defined as an optimization problem. Three approaches are presented here. Denote by $E(\cdot)$ the mean value, the first approach is given as to minimize the mean value of the GDI

$$\min_{\Omega} \ (E(\text{GDI})) \tag{19}$$

meaning that the average dynamic change of the GDI is minimized. This approach is useful when the overall dynamics needs to be adjusted. The second approach is to minimize the standard deviation

$$\min_{\Omega} \ (SD(\text{GDI})) \tag{20}$$

where $SD(\cdot)$ indicates the standard deviation. Equation (2) shows that the dynamic variation is minimized, which is the main concern of dynamic balancing. The third approach is to minimize the maximum value of the GDI over the region considered

$$\min_{\Omega} \ (\max(\text{GDI})) \tag{21}$$

The goal of this approach is to minimize the bound of the GDI, the similar effect to the second approach. Based on the nature of the problem under study, one can use one of three approaches or their combinations to perform dynamic balancing.

4.3 Relationship between kinematic and dynamic characteristics

Before giving examples to demonstrate the proposed dynamic balancing method, it may be worthwhile to mention the relationship between the hexapod kinematic and dynamic characteristics. By referring to equation (10), one can see that the hexapod generalized inertia matrix **D** consists of two parts, namely, the Jacobian **J** and the inertia matrix **M**.

The inertia matrix **M** is constant, as defined in the moving platform coordinates, and has no contribution to variation in **D**. It is the Jacobian **J** that causes **D** to vary with the hexapod configurations, implying that geometric design of the hexapod is important in terms of dynamic balancing. Though a number of geometric design methods were put forward in the literature, there has been no discussion regarding the effect on the dynamic balancing. Due to the limitation of the paper, this problem will be addressed in a separate paper.

Isotropy of **D** is affected by **M** and **J**, and it is obvious that if **M** and **J** are isotropic, then **D** is isotropic. The kinematic isotropy, i.e. isotropic **J**, has been addressed in the literature.[17] For achieving isotropic **M** a sphere type of the tool holder may be more applicable. This will be the subject of the future research.

5. CASE STUDIES

5.1 System description

The geometric structure of the hexapod under study is given in Figure 2. Its base and moving platform are made of hexagon shape. The origins of the global coordinates attached to the base and the moving plate coordinates are set at the centroid of the hexagons. The coordinates of the connecting passive joints on the base and platform are defined with respect to the origins of the respective coordinates, and the details are given in Appendix A. The moment of the inertia of a hexagon shape was derived using the symbolic package, Maple, and the results are given in Appendix B.

5.2 Task definition

To demonstrate the proposed method, we define a task probability function as a sphere within the hexapod's workspace. Inside the sphere, it is assumed that the task probability is uniformly distributed, and only the position is of concern. Then this probability function can be given as

$$\mathrm{p}(\mathbf{x}_\mathrm{p}) = \begin{cases} \dfrac{3}{4\pi \mathrm{b}^3} & \|\mathbf{x}_\mathrm{p}\| \le \mathrm{b} \\ 0 & \text{elsewhere} \end{cases} \tag{22}$$

where b is the radius of the sphere, and $\mathbf{x}_\mathrm{p}$ is the position vector.

For a selected global dynamic index (GDI), the mean value can be obtained as

$$E[\text{GDI}] = \int_\Omega \text{GDI}(\mathbf{x}_\mathrm{p}) p(\mathbf{x}_\mathrm{p}) \mathrm{d}\Omega \tag{23}$$

and the standard deviation can be given as

$$SD[\text{GDI}] = \sqrt{\int_\Omega ([\text{GDI}(\mathbf{x}_\mathrm{p}) - E[\text{GDI}])^2 p(\mathbf{x}_\mathrm{p}) \mathrm{d}\Omega} \tag{24}$$

Also, the bound of the GDI can be determined as

$$\max(\text{GDI}(\mathbf{x}_\mathrm{p})) \tag{25}$$

https://doi.org/10.1017/S0263574799001484 Published online by Cambridge University Press

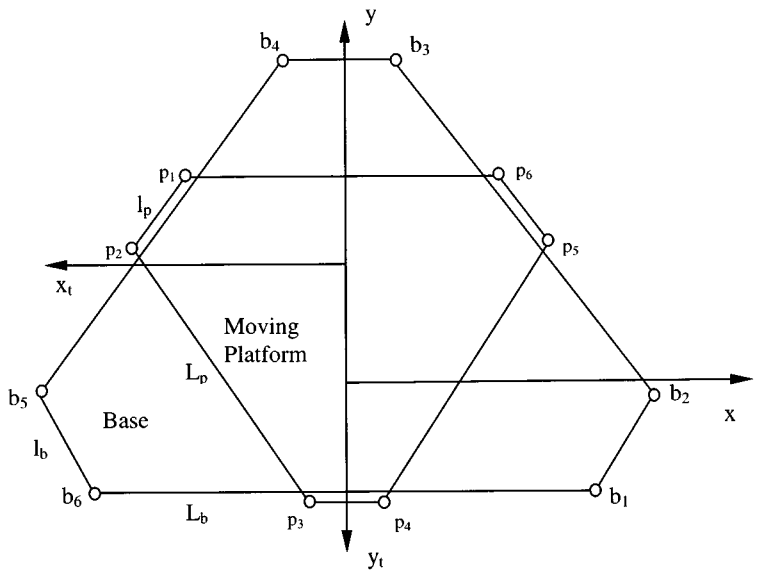

Fig. 2. Geometry of the base and the moving platform.

5.3 Implementation

For the purpose of dynamic balancing, we propose here to use the tool holder attached to the moving platform as the hexapod's balancing counterweight. Denote by m^* the counterweight of the tool holder, and by $\mathbf{r}$ its center of mass in the moving platform coordinates; consider that the tool holder has an initial weight m_o, and the total weight is $m = m_o + m^*$, then the problem of dynamic balancing is to find m^* and $\mathbf{r}$.

For the comparison purpose, three isotropic measures given in Section 3.2 namely, $\sigma(\mathbf{D})$, $\gamma(\mathbf{D})$ and DCI, are used. For better dynamic performance, it is required to maximize the first two. To follow the standard approach of minimization, the following conversion is made for the first two indices

$$\max_{(\mathbf{r},m^*);\mathbf{x}_p\in\Omega}(\sigma(\mathbf{D}(\mathbf{x}_p; m^*, \mathbf{r}))) \Rightarrow \min_{(\mathbf{r},m^*);\mathbf{x}_p\in\Omega}(\kappa(\mathbf{D}(\mathbf{x}_p; m^*, \mathbf{r}))) \quad (26)$$

and

$$\max_{(\mathbf{r},m^*);\mathbf{x}_p\in\Omega}(\gamma(\mathbf{D}(\mathbf{x}_p; m^*, \mathbf{r}))) \Rightarrow \min_{(\mathbf{r},m^*);\mathbf{x}_p\in\Omega}(-\gamma(\mathbf{D}(\mathbf{x}_p; m^*, \mathbf{r}))) \quad (27)$$

For the third index, it is defined as

$$\min_{(\mathbf{r},m^*);\mathbf{x}_p\in\Omega}(\mathrm{DCI}(\mathbf{x}_p; m^*, \mathbf{r})) \quad (28)$$

For each GDI considered, three approaches defined in equations (19) to (21) are implemented. For optimization, m^* and $\mathbf{r} = [r_x, r_y, r_z]^T$ are constrained as below

$$m^* \geq 0;$$
$$r_x = 0;$$
$$-0.3 \leq r_y \leq 0.3;$$

and

$$-0.3 \leq r_z \leq 0.3$$

The geometric and material parameters are given as $L_b = 1.0$m, $l_b = 0.05$m, $L_p = 0.5$m, $l_p = 0.03$m, t (thickness) $= 0.1$m, ρ (density) $= 8000$ kg/m^3. In the simulation, the initial value of $\mathbf{r}$ and m^* are $\mathbf{r}_o = [0, -0.3, -0.3]^T$ and $m_o^* = 10$.

Tables II to X show the simulation results. It is recalled that for the symbols used in these tables, b is the radius of the sphere region, r_y and r_z are the components of the center of the tool holder (note that $r_x = 0$), m^* is the counterweight. Tables 2–4 are the results of $\kappa(\mathbf{D})$ considering $E[\kappa(\mathbf{D})]$,

Table II. Results of min $E[\kappa(\mathbf{D})]$.

b	r_y	r_z	m^*	$E[\kappa(\mathbf{D})]$	Corresponding $SD[\kappa(\mathbf{D})]$
0.05	−0.3	0.000	6.9575	5.6915	0.5382
0.15	−0.3	−0.0003	11.3329	7.1936	1.56525
0.25	−0.3	−0.0002	18.3668	10.4994	4.4653
0.35	−0.3	0.0000	48.6977	25.5267	37.025

Table III. Results of min $SD[\kappa(\mathbf{D})]$.

b	r_y	r_z	m^*	$SD[\kappa(\mathbf{D})]$	Corresponding $E[\kappa(\mathbf{D})]$
0.05	0.1743	−0.0059	4.9064	0.0314	6.8366
0.15	−0.3	0.1096	25.5053	1.0833	9.243
0.25	−0.3	−0.0540	49.3229	3.9970	11.882
0.35	−0.2992	−0.0002	63.5916	34.571	25.804

Table IV. Results of min $max[\kappa(\mathbf{D})]$.

b	r_y	r_z	m^*	$max[\kappa(\mathbf{D})]$
0.05	0.2208	−0.0006	0	2.5635
0.15	0.3	−0.0515	7.6033	3.18276
0.25	0.3	0.000	46.9189	4.38654
0.35	−0.3	0.0000	62.8524	40.0499

https://doi.org/10.1017/S0263574799001484 Published online by Cambridge University Press

Table V. Results of min $E[-\gamma(\mathbf{D})]$.

b	r_y	r_z	m*	$E[-\gamma(\mathbf{D})]$	Corresponding $SD[-\gamma(\mathbf{D})]$
0.05	−0.0278	0.0237	0	0.1954	0.0014
0.15	−1.155e−5	−1.104e−5	0	0.1921	0.0056
0.25	2.161e−5	−3.605e−5	0	0.1850	0.0136
0.35	−1.256e−5	4.415e−5	0	0.1729	0.0288

$SD[\kappa(\mathbf{D})]$ and $max[\kappa(\mathbf{D})]$. Tables 5–7 are the results of $\gamma(\mathbf{D})$ considering $E[-\gamma(\mathbf{D})]$, $SD[-\gamma(\mathbf{D})]$ and $max[-\gamma(\mathbf{D})]$. Tables VIII–X are the results of DCI considering E[DCI], SD[DCI] and max[DCI]. In all the simulation cases, the sphere region is varied by radius b in order to investigate its effect.

Observations can be made from Tables II to X. In terms of three approaches, i.e. min E, min SD and minmax, the

Table VI. Results of min $SD[-\gamma(\mathbf{D})]$.

b	r_y	r_z	m*	$SD[-\gamma(\mathbf{D})]$	Corresponding $E[-\gamma(\mathbf{D})]$
0.05	0.3	0.3	10.0	0.0209	0.1772
0.15	−4.884e−6	−1.55e−6	0	0.0262	0.2168
0.25	2.242e−6	−2.005e−6	0	0.0284	0.2094
0.35	0.3	0.3	1000	0.0097	0.0508

Table VII. Results of min $max[-\gamma(\mathbf{D})]$.

b	r_y	r_z	m*	$max[-\gamma(\mathbf{D})]$
0.05	−9.6559e−4	−6.237e−5	0	0.1929
0.15	1.527e−6	−1.116e−6	0	0.1787
0.25	4.318e−3	−3.732e−4	0	0.1488
0.35	2.696e−5	−2.910e−5	0	0.0894

Table VIII. Results of min $E[\kappa(\mathbf{D})]$.

b	r_y	r_z	m*	E[DCI]	Corresponding SD[DCI]
0.05	−0.3	−0.3	0.3534	719.71	7.9035
0.15	0.3	0.3	0	913.8049	16.7462
0.25	0.2188	−0.3	0	1907.9	19.6910
0.35	0.0462	0	0	4154.3	830.412

Table IX. Results of min SD[DCI].

b	r_y	r_z	m*	SD[DCI]	Corresponding E[DCI]
0.05	0.0	0.0	0.0	7.7730	966.63
0.15	−0.3	−0.3	41.3197	8.5195	2473.5
0.25	−0.3	−0.3	15.816	7.8249	3091.5
0.35	−4.506e−6	−9.42e−6	0	830.31	4154.4

Table X. Results of min max[DCI].

b	r_y	r_z	m*	max(DCI)
0.05	−0.3	0.3	0	939.18
0.15	0.3	0.3	0	1656.9
0.25	0.1026	−0.1948	0	7737.2
0.35	0.1871	0.055	0	6352.8

increasing values of the counterweight m* are produced as the sphere region increases, and the center of mass always varies. For the comparison purpose, SD corresponding to min E, and vice versa are calculated, and interestingly the optimal value of min E is in the same magnitude of E obtained from min SD, and so is the other around. However, and the optimization results are relatively close for $\kappa(\mathbf{D})$, but not for the other indices.

In terms of three measures, i.e. $\kappa(\mathbf{D})$, $-\gamma(\mathbf{D})$ and DCI, the last two intend to apply a zero counterweight, however, the center of mass always varies.

6. CONCLUDING REMARKS

In this paper, a method for hexapod dynamic balancing has been discussed. The method is based on the concept of minimization of the hexapod inertia change by utilising the tool holder attached to the end-effector as a counterweight. The global dynamic index (GDI) has been put forward using the task probability function. Three approaches are proposed including minimization of the mean value, the standard deviation and the bound. Examples are provided to demonstrate the proposed method.

ACKNOWLEDGEMENT

The author wishes to thank Dr. S. Xu for his assistance in implementing the optimization programs in Matlab.

References

1. U. Heisel, and M. Gringel, "Machine tool design requirements for high-speed machining," *Annals of the CIRP* **45**(1), 389–392 (1996).
2. D. Stewart, "A platform with six degrees of freedom" *Proceedings of the Institution of Mechanical Engineers* **180**, No. 5, 371–378 (1965).
3. J.L. Overholt and A.A. Zeid, "Partial state feedback linearized based control for a steward platform" *Proceedings of the 1991 Summer Computer Simulation Conference* (1991) pp. 512–517.
4. The UH IfA Detector Lab, Wed site home page (1998).
5. T. Tanikawa, T. Arai and T. Masuda, "Development of micro manipulation system with two-finger micro hand" *Proceedings of IROS 96*, (1996) pp. 850–855.
6. M. Suzuki, K. Watanabe, T. Shibukawa, T. Tooyama and K. Hattori, "Development of milling machine with parallel mechanism" *Toyota Technical Review*, Vol. 47, No. 1, pp. 125–130 (1997).
7. H. Ouyang, C. Mechefske and F. Xi, "Effect of the leg errors on hexapod location accuracy" *COMADEM 98* (1998).
8. K.H. Hunt, *Kinematic Geometry of Mechanisms* (Clarendon Press, Oxford 1978).
9. C.F. Earl and J. Rooney, "Some kinematics structures for robot manipulator design" *ASME Journal of Mechanisms, Transmissions, and Automation in Design* **105**, 15–22 (1983).

https://doi.org/10.1017/S0263574799001484 Published online by Cambridge University Press

10. G. Pritschow and W. Philip, "Direct drives for high dynamic machine tool axes" *Annals of the CIRP* **41**(1) 441–415 (1992).
11. F. Pierrot, A. Fournier and P. Dauchez, "Towards a fully-parallel 6 DOF robot for high-speed applications" *Proceedings of the 1991 IEEE ICRA*, (1991) pp. 1288–1293.
12. F. Behi, "Kinematic analysis for six-degree-of-freedom 3-PRPs parallel mechanism" *IEEE Transactions on Robotics and Automation* **3**, No. 3, 561–565 (1988).
13. L–W. Tsai, "Systematic Enumeration of Parallel Manipulators" *ISR Technical Research Report* (The University of Maryland, 1998).
14. E.F. Fitcher, "A Stewart platform-based manipulator: general theory and practical construction" *Int. J. Robotics Research* **5**, No. 2, 157–182 (1986).
15. K. Sugimoto, "Kinematic and dynamic analysis of parallel manipulators by means of motor algebra" *J. Mechanisms, Transmissions, and Automation in Design* 109, 3–7 (1987).
16. J–P. Merlet, "Singular configurations of parallel manipulators and Grassman geometry" *Int. J. Robotics Research* **8**, No. 5, 45–56 (1989).
17. C. Gossselin and J. Angeles, "The optimum kinematic design of a planar three-degree-of-freedom parallel manipulator" *Mechanisms, Transmissions, and Automation in Design* **110**, 35–41 (1988).
18. R.S. Stoughton and T. Arai, "A modified Stewart platform manipulator with improved dexterity" *IEEE Transactions on Robotics and Automation* **9**, No. 2, 166–173 (1993).
19. H. Asada and J.–J.E. Slotine, *Robot Analysis and Control* (John Wiley and Sons, New York, 1985).
20. J.Y.S. Luh, M.W. Walker and R.P.C. Paul, "On-line computational scheme for mechanical manipulators" *ASME Journal of Dynamic Systems, Measurements, and Control* **102**, 102–110 (1980).
21. M.W. Walker, "Adaptive control of manipulators containing closed kinematic loops" *IEEE Transactions on Robotics and Automation* **6**, No. 1, 10–19 (1990).
22. Geodetic, *Hexapod: the technology breakthrough* (Geodetic Technology Ltd., UK, 1996).
23. F. Xi and R.G. Fenton, "Modeling and analysis of flexible link manipulators using the algebra of rotations" *IEEE Transactions on Systems, Man, and Cybernetics* **24**, No. 7, 1022–1034 (1994).
24. J–P. Merlet, "Direct kinematics and assembly modes of parallel manipulators" *Int. J. Robotics Research* **11**, No. 2, 150–162 (1992).
25. J–P. Merlet, "Closed-form resolution of the direct kinematics of parallel manipulators using extra sensors data" *Proceedings of the 1993 IEEE IRCA* (1993) pp. 200–204.
26. Ji Zhiming, "Dynamics decomposition for Stewart platform" *J. Mechanical Design* **116**, 67–69 (1994).
27. M. Raghavan and B. Roth, "On the design of manipulators for applying wrenches" *Proceedings of the 1989 IEEE International Conference on Robotics and Automation* (1989) pp. 438–443.
28. M. Jean and C. Gosselin, "Static balancing of planar parallel manipulators" *Proceedings of the 1996 IEEE International Conference on Robotics and Automation* (1996) pp. 3732–3737.
29. R.S. Berkof and G.G. Lowen, "A new method for completely force balancing simple linkages" *J. Engineering of Industry, Transactions of the ASME*, **91B**, 21–26 (1969).
30. C. Bagci, "Complete shaking force and shaking moment balancing of link mechanisms using balancing idler loops" *ASME Journal of Mechanical Design* **104**, 482–493 (1982).
31. J.R. Singh and J.R. Rastegar, "Optimal synthesis of robot manipulators based on global dynamic parameters" *Int. J. Robotics Research* **11**, No. 6, 538–548 (1992).
32. H. Asada, "A geometrical representation of manipulator dynamics and its application to arm design" *ASME Journal of Dynamic Systems, Measurement and Control* **105**, 131–135 (1983).
33. O. Ma and J. Angeles, "Optimum design of manipulators under dynamic isotropy conditions" *Proceedings of the 1993 IEEE IRCA* (1993) pp. 470–475.
34. G.J. Wien, R.A. Scott and M.Y. Zarrugh, "The role of inertia sensitivity in the evaluation of manipulator performance" *ASME Journal of Dynamic Systems, Measurement and Control* **111**, No. 2, 194–199 (1989).

APPENDIX A CONNECTING JOINT COORDINATES

Denote by L_b and l_b the long and short side of the base hexagon, respectively, according to the label given in Figure 2, the connecting joint coordinates of the base are given below

b_1: $[L_b/2,\ -y_b,\ 0]$
b_2: $[(L_b+l_b)/2,\ l_b\times c_s - y_b,\ 0]$
b_3: $[l_b/2,\ (L_b+l_b)\times c_s - y_b,\ 0]$
b_4: $[-l_b/2,\ (L_b+l_b)\times c_s - y_b,\ 0]$
b_5: $[-(L_b+l_b)/2,\ l_b\times c_s - y_b,\ 0]$
b_6: $[-L_b/2,\ -y_b,\ 0]$

where $c_s = \cos(30°)$, and $y_b = (L_b/2 + l_b)\times \mathrm{tg}(30°)$. Likewise, the connecting joint coordinates of the moving platform are given as

${}^tp_1$: $[L_p/2,\ -y_p,\ 0]$
${}^tp_2$: $[(L_p+1_p)/2,\ l_p\times c_s - y_p,\ 0]$
${}^tp_3$: $[l_p/2,\ (L_p+l_p)\times c_s - y_p,\ 0]$
${}^tp_4$: $[-l_p/2,\ (L_p+l_p)\times c_s - y_p,\ 0]$
${}^tp_5$: $[-(L_p+l_p)/2,\ l_p\times c_s - y_p,\ 0]$
${}^tp_6$: $[-L_p/2,\ -y_p,\ 0]$

where $y_p = (L_p/2 + l_p)\times \mathrm{tg}(30°)$, and L_p and l_p are the long and short side of the platform hexagon, respectively.

APPENDIX B MOMENT OF INERTIA OF A HEXAGON

Denote by L and l the long and short side of a hexagon, the moment of inertia along x, y and z axis is given as

$$I_{xx} = \sqrt{3}\left(\frac{1}{96}L^4 - \frac{5}{32}l^4 + \frac{1}{4}Ll^3 - \frac{1}{8}L^2l^2\right)$$

$$I_{yy} = \sqrt{3}\left(\frac{1}{96}L^4 - \frac{5}{32}l^4 + \frac{1}{4}Ll^3 - \frac{1}{8}L^2l^2\right)$$

$$I_{zz} = I_{xx} + I_{yy}$$

https://doi.org/10.1017/S0263574799001484 Published online by Cambridge University Press